J|A|C|S
ARTICLES

Published on Web 01/27/2010

Positive Charge States and Possible Polymorphism of Gold Nanoclusters on Reduced Ceria

Changjun Zhang,[†,‡] Angelos Michaelides,[‡] David A. King,[†] and Stephen J. Jenkins*[,†]

Department of Chemistry, University of Cambridge, Lensfield Road, Cambridge CB2 1EW, United Kingdom, and London Centre for Nanotechnology & Department of Chemistry, University College London, London WC1H 0AH, United Kingdom

Received August 7, 2009; E-mail: sjj24@cam.ac.uk

Abstract: The catalytic properties of Au/CeO_2 systems are sensitive to the nature of Au clusters; however, atomic information on Au clusters is sparse. In this work, we use density functional theory to investigate the nucleation of small Au clusters (up to Au_{11}). By depositing Au atoms one by one at a reduced CeO_2{111} surface, we present detailed nucleation patterns. Although relatively small in size, the nanoclusters obtained exhibit interesting characteristic features. In addition to the face-centered cubic (fcc) geometry, reminiscent of bulk Au, we also find the existence of novel hexagonal close-packed (hcp) structures. Furthermore, the facets of the nanoclusters are versatile, comprising {111}/{100} combinations for the fcc-like clusters and $\{10\bar{1}1\}$/{0001} combinations for the hcp-like. Electronically, the contact layer Au atoms that bond with surface O atoms are positively charged, which could have significant implications in catalysis.

1. Introduction

Ceria-supported gold clusters have recently attracted much research attention, primarily due to their excellent activities for the low-temperature water−gas shift (WGS) reaction, which is a crucial step in many applications including the production of hydrogen for fuel cells.[1−3] Despite extensive studies, some fundamental issues remain disputed, such as the catalytic roles of the Au and the ceria support and the relative importance of different WGS reaction mechanisms.[4] The existence of such controversies is not entirely surprising, as the catalytic properties of Au/CeO_2 systems are sensitive to the nature of Au clusters. CO adsorption (i.e., one of the initial processes in the WGS reaction) may be taken as a simple example: the molecule adsorbs more strongly on less-coordinated corner sites, which are more abundant on smaller clusters, whereas the adsorption at edge or terrace sites, which are more abundant on larger clusters, is less strong.[5,6] Another example is the WGS reaction mechanism itself, which also has a strong dependence on the size and shape of the clusters. Theoretical studies on Au_4/CeO_2{111}, Au_3/CeO_2{111}, and Au_{29} systems showed distinctly different reaction paths[7−9] (e.g., the formate mechanism versus the associative carboxyl mechanism[10,11]) and different rate-determining elementary steps.

In addressing the catalytic properties of Au/CeO_2 systems, detailed knowledge of Au structure is undoubtedly of great importance. Several experiments were carried out to characterize the clusters on CeO_2{111}.[12−14] The consensus from those studies is that Au exhibits a three-dimensional growth model, the shape of Au clusters is hemispherelike, and clusters are well-faceted with the top facet possessing a hexagonal shape suggesting a {111} surface. There is also a suggestion that the side facet of the clusters has a {100} feature.[13] In addition, it was proposed that Au preferentially nucleates at defects of the support and the clusters are fairly stable toward sintering.[12] On the theory side, however, the study of Au clusters on ceria is scarce. WGS pathways have been studied on Au_3 and Au_4 clusters (both on ceria) and on a pure Au_{29} cluster.[7−9] However, there has been so far no theoretical study concerning Au nucleation, and structures of Au clusters on ceria have not been established yet. In this work, we carry out a density functional theory (DFT) study on the nucleation of small Au clusters on ceria, which provides atomic insights into the structural properties of the clusters. This work builds on our previous studies on reduced CeO_2{111} surfaces and singly adsorbed Au on the surfaces.[15−17]

[†] University of Cambridge.
[‡] University College London.

(1) Fu, Q.; Saltsburg, H.; Flytzani-Stephanopoulos, M. *Science* **2003**, *301*, 935.
(2) Deluga, G. A.; Salge, J. R.; Schmidt, L. D.; Verykios, X. E. *Science* **2004**, *303*, 993.
(3) Park, S.; Vohs, J. M.; Gorte, R. J. *Nature* **2000**, *404*, 265.
(4) See a review by Burch, R. *Phys. Chem. Chem. Phys.* **2006**, *8*, 5483.
(5) Weststrate, C. J.; Resta, A.; Westerström, R.; Lundgren, E.; Mikkelsen, A.; Andersen, J. N. *J. Phys. Chem. C* **2008**, *112*, 6900.
(6) Yim, W.-L.; Nowitzki, T.; Necke, M.; Schnars, H.; Nickut, P.; Biener, J.; Biener, M. M.; Zielasek, V.; Al-Shamery, K.; Klüner, T.; Bäumer, M. *J. Phys. Chem. C* **2007**, *111*, 445.
(7) Liu, Z.; Jenkins, S. J.; King, D. A. *Phys. Rev. Lett.* **2005**, *94*, 196102.
(8) Chen, Y.; Hu, P.; Lee, M.-H.; Wang, H. *Surf. Sci.* **2008**, *602*, 1736.
(9) Liu, P.; Rodriguez, J. A. *J. Chem. Phys.* **2007**, *126*, 164705.
(10) Shido, T.; Iwasawa, Y. *J. Catal.* **1992**, *136*, 493.
(11) Shido, T.; Iwasawa, Y. *J. Catal.* **1993**, *141*, 71.
(12) Lu, J.-L.; Gao, H.-J.; Shaikhutdinov, S.; Freund, H.-J. *Catal. Lett.* **2007**, *114*, 8.
(13) Akita, T.; Okumura, M.; Tanaka, K.; Kohyama, M.; Haruta, M. *J. Mater. Sci.* **2005**, *40*, 3101.
(14) Weststrate, C. J.; Resta, A.; Westerström, R.; Lundgren, E.; Mikkelsen, A.; Andersen, J. N. *J. Phys. Chem.* **2008**, *112*, 6900.
(15) Zhang, C.; Michaelides, A.; King, D. A.; Jenkins, S. J. *Phys. Rev. B* **2009**, *79*, 075433.

2. Methodology

We carry out spin-polarized calculations within the DFT framework, as implemented in the Vienna ab initio simulation program (VASP), a plane-wave pseudopotential DFT package.[18−20] We use the projector-augmented wave method to describe the effect of the core electrons on the valence electrons in the system.[21,22] The Ce 5s, 5p, 5d, 4f, and 6s electrons, the O 2s and 2p electrons, and the Au 5d, 6s, and 6p electrons are treated as valence electrons. For the electron exchange−correlation functional, the generalized gradient approximation (GGA) of Perdew and Wang[23] is used. It is known that the stability of pure Au clusters, in particular the transition between the planar (2D) and three-dimensional (3D) structures, is sensitive to the choice of density functional. At surfaces, however, the issue may not be acute because of the influence exerted by the surface on the clusters. This is demonstrated in the Supporting Information, where calculations on a series of Au clusters on ceria with the PBEsol functional are reported. By comparing results obtained from different functionals, we find that the general trend of stabilities remains the same. In all the calculations, we choose the DFT+U methodology,[24,25] which has been shown to be essential in descriptions of reduced ceria systems.[26] In this approach, the Hubbard parameter, U, is introduced to account for the strong on-site Coulomb repulsion among the localized Ce 4f electrons. The value of the U term is chosen to be 5.0 eV, which is the same as (or close to) that used in many previous studies on ceria systems.[27−33] We note that some authors use GGA+U ($U = 3$ eV) with the lattice parameters calculated with LDA+U ($U = 5$ eV) to study ceria surfaces.[34] This is questionable, particularly in studying the reduced $CeO_2\{111\}$ surface, because previous studies showed that GGA+U ($U = 3$ eV) would lead to electron delocalization in those situations,[15,31] which is a physically incorrect behavior. Furthermore, the lattice parameters calculated with LDA+U ($U = 5$ eV) are smaller (by ~1.3%) than those calculated with GGA+U, a fact that would actually facilitate further the electron delocalization.

The $CeO_2\{111\}$ surface terminates in stoichiometric O−Ce−O trilayers stacked along a ⟨111⟩ direction and is the thermodynamically most stable facet. A (3×3) unit cell is mainly chosen in studying the Au nucleation. For some large clusters, a (4×4) unit cell is also used in order to minimize the interaction between cells. We find that although there are some energy differences from the calculations conducted in the two different cells, the main geometrical and electronic features obtained are very similar. The slab used in the calculations has nine atomic layers, which is a common choice in studying the $CeO_2\{111\}$ surface.[32−34] The vacuum regions for the slabs are generally around 12 Å. During structure optimizations atoms are allowed to relax until the forces are smaller than 0.01 eV/Å, except those in the lowest three layers that are constrained to the equilibrium positions calculated for the defect-free supercell. The sampling of the Brillouin zone was performed with a $2 \times 2 \times 1$ Monkhorst−Pack k-point mesh, and the number of plane waves used to expand the Kohn−Sham orbitals is controlled by a cutoff energy of 400 eV, which is sufficient to obtain converged results.

In the Au nucleation, we position one Au atom at a time at the surface, followed at each stage by a geometry optimization. We note, however, that when the Au clusters become large, there would be too many possible geometries to be taken fully into account. Thus, to investigate Au_x (x is the number of Au atoms), we only choose several most stable (or most representative) geometries found for Au_{x-1} as the starting configurations and subsequently search for the stable geometries of the newly arrived xth Au atom. This procedure is repeated until Au_{10} or Au_{11} clusters form. Although this method may not categorically produce *the* most stable Au_x cluster, we consider that the clusters obtained are certainly representative. We also note that Au_{10} (or Au_{11}) is the largest and the most stable cluster that can be studied in the (3×3) unit cell; larger clusters would need a larger unit cell (and thus much larger computational effort) to accommodate them. However, the study of Au_{10} or Au_{11} clusters, albeit relatively small in size, does reveal some interesting and characteristic structural features, as will be seen later.

We should also mention that adding one Au atom at a time in our calculations is not inconsistent with the usual experimental preparation method for Au nanoparticles (i.e., the deposition precipitation method or the vapor deposition method).[1,12,13] Of course, an alternative calculation strategy could be to position a Au cluster somewhere above the surface, followed by a dynamics simulation to locate the energy minima. However, the choice of shape for the cluster would be quite arbitrary, not to mention the greater cost of dynamics calculations in comparison to static ones. That being said, we have performed dynamics calculations on the two Au_{10} clusters obtained from our static calculations, in order to check their stabilities (to be discussed below). Another point of note in our calculation is the spin distribution on Ce ions. Typically, our calculations are carried out with two or three different initial spin arrangements. In all cases, the total energy differences are small and the effects on the averaged Au adsorption energy are negligible, which is consistent with previous calculations on surfaces and singly adsorbed Au.[15−17] Thus, we did not attempt to exhaust all the possibilities for spins.

3. Results and Discussion

The formation of Au clusters is believed to be seeded at Au atoms embedded into the ceria lattice, so that the clusters can be resistant to sintering and do not lose their integrity during reactions.[1,4] The intimate contact between the cluster and the surface suggests that the former must anchor at surface defects. Meanwhile, ceria is well-known for its remarkable O-storage capability,[35] that is, the ability to undergo rapid redox cycles by releasing and storing O, implying that O vacancies are always present. Furthermore, there is also experimental evidence to suggest the importance of O vacancies in Au/CeO_2 catalysts. For example, Wang et al.[36] observed a Ce^{3+} peak in synchrotron-based photoemission spectra, indicative of the presence of O

(16) Zhang, C.; Michaelides, A.; King, D. A.; Jenkins, S. J. *J. Chem. Phys.* **2008**, *129*, 194708.
(17) Zhang, C.; Michaelides, A.; King, D. A.; Jenkins, S. J. *J. Phys. Chem. C* **2009**, *113*, 6411.
(18) Kresse, G.; Hafner, J. *Phys. Rev. B* **1994**, *49*, 14251.
(19) Kresse, G.; Furthmüller, J. *Comput. Mater. Sci.* **1996**, *6*, 15.
(20) Kresse, G.; Furthmüller, J. *Phys. Rev. B* **1996**, *54*, 11169.
(21) Blöchl, P. E. *Phys. Rev. B* **1994**, *50*, 17953.
(22) Kresse, G.; Joubert, D. *Phys. Rev. B* **1999**, *59*, 1758.
(23) Perdew, J. P. In *Electron Structure of Solids '91* ; Ziesche, P., Eschrig, H., Eds.; Akademie Verlag: Berlin, 1991.
(24) Anisimov, V. I.; Zaanen, J.; Andersen, O. K. *Phys. Rev. B* **1991**, *44*, 943.
(25) Rohrbach, A.; Hafner, J.; Kresse, G. *J. Phys.: Condens. Matter* **2003**, *15*, 979.
(26) Ganduglia-Pirovano, M. V.; Hofmann, A.; Sauer, J. *Surf. Sci. Rep.* **2007**, *62*, 219.
(27) Kresse, G.; Blaha, P.; Da Silva, J. L. F.; Ganduglia-Pirovano, M. V. *Phys. Rev. B* **2005**, *72*, 237101.
(28) Da Silva, J. L. F.; Ganduglia-Pirovano, M. V.; Sauer, J.; Bayer, V.; Kresse, G. *Phys. Rev. B* **2007**, *75*, 045121.
(29) Andersson, D. A.; Simak, S. I.; Jahansson, B.; Abrikosov, I. A.; Skorodumova, N. V. *Phys. Rev. B* **2007**, *75*, 035109.
(30) Castleton, C. W. M.; Kullgren, J.; Hermansson, K. *J. Chem. Phys.* **2007**, *127*, 244704.
(31) Nolan, M.; Grigoleit, S.; Sayle, D. C.; Parker, S. C.; Watson, G. W. *Surf. Sci.* **2005**, *576*, 217.
(32) Fabris, S.; Vicario, G.; Balducci, G.; de Gironcoli, S.; Baroni, S. *J. Phys. Chem. B* **2005**, *109*, 22860.
(33) Herschend, B.; Baudin, M.; Hermansson, K. *J. Chem. Phys.* **2007**, *126*, 234706.
(34) Castellani, N. J.; Branda, M. M.; Neyman, K. M.; Illas, F. *J. Phys. Chem. C* **2009**, *113*, 4948.
(35) Trovarelli, A. *Catal. Rev. Sci. Eng.* **1996**, *38*, 439.

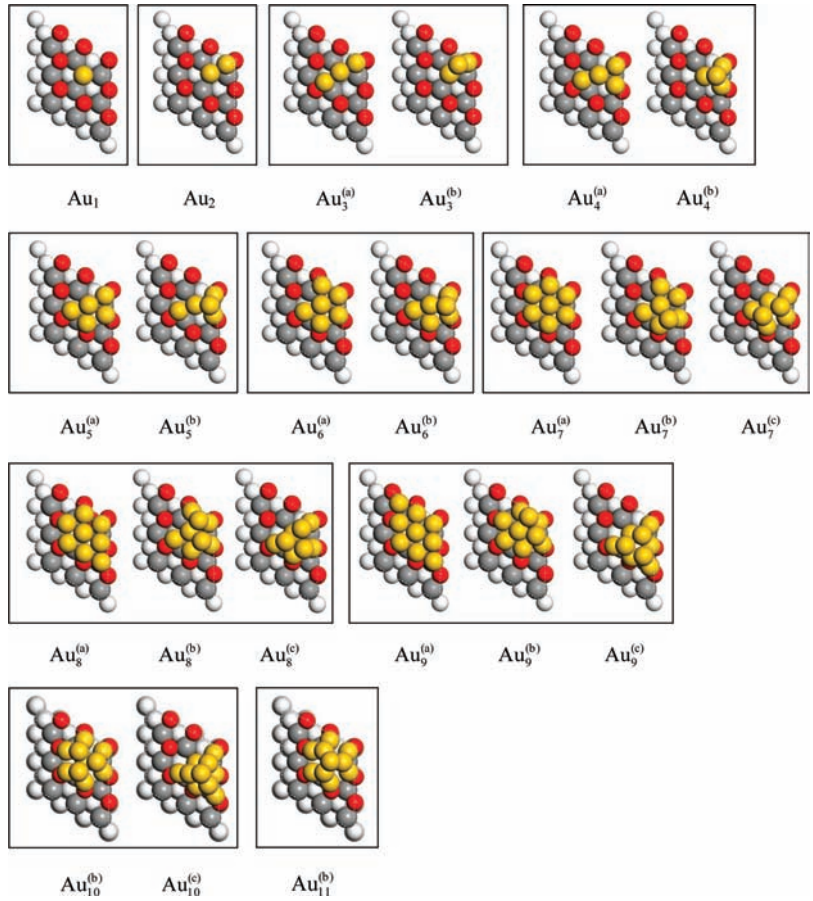

Figure 1. Nucleation of Au clusters (top views). Au, O, and Ce atoms are in gold, red, and gray respectively. In black and white print, the atoms can be distinguished by their sizes. The first and second layers of the substrate are O and Ce layers, respectively; for clarity, the remaining substrate is shown in white.

vacancies, and they further showed that, under WGS conditions, the active sites should involve small Au clusters in close contact with O vacancies. From our recent studies,[7,16] we have shown clearly that, under WGS conditions, Au prefers an O vacancy site at a reduced CeO_2{111} surface to any site at the perfect surface. When all this is taken into account, it is therefore reasonable to consider that the O vacancy is the Au nucleation site. We note that, in addition to the single vacancy, O vacancy clusters could also be the Au nucleation sites;[15,37,38] however, these are neglected in this work due to their complexity. Besides, we also neglect the Ce vacancy that was suggested to be the anchoring site for Au clusters from some studies;[39] this suggestion is likely to be incorrect, because under WGS reaction conditions, O vacancies are much easier to form and much more stable than Ce vacancies, and Au strongly prefers the O vacancy site to the Ce vacancy site, as we showed in a recent study.[17]

3.1. Nucleation of Au_x ($x = 1-11$). Starting with the {111} surface at which an O vacancy presents, the nucleation has been modeled sequentially. As schematically shown in Figure 1, the first Au atom (Au_1) adsorbs at the O vacancy position: it sits ~1.3 Å above the surface (with respect to the averaged position of the surface O atoms) and the Au−Ce distances are ~3.2 Å. To illustrate the adsorption strength, we report in this section the averaged adsorption energy (ΔE_x^{av}), which can be expressed as

$$\Delta E_x^{av} = (E_{slab}^{Au_x} - E_{slab} - xE_{Au})/x \quad (1)$$

where $E_{slab}^{Au_x}$, E_{slab}, and E_{Au} are energies of Au_x/CeO_2, the pure surface, and an isolated Au atom, respectively. Thus, for a given number of Au atoms (x), ΔE_x^{av}shows the relative stability for possible Au_x structures that could form via different growth mechanisms. For Au_1, we found that the adsorption at the vacancy site is much stronger than that at the perfect surface: ΔE_1^{av} is −2.25 eV for the former and −1.14 eV for the latter.

The second Au atom sits beside the first one, and it also forms a bond with a neighboring O atom (2.12 Å bond distance). Such a geometry is much more favorable than one with the second Au atom sitting directly above the first without bonding to any surface atom, although ΔE_2^{av} (−2.08 eV) is somewhat less negative than ΔE_1^{av}.

For Au_3, there are several ways to arrange the Au atoms at the surface. In Figure 1 we show only the two most stable configurations: (i) the third Au atom, like the second one, also sits beside the first Au atom and forms an extra bond with a neighboring O atom [denoted as $Au_3^{(a)}$]; (ii) the third Au atom sits above the first two Au atoms, forming no bond with any surface O [denoted as $Au_3^{(b)}$]. These two configurations may be viewed as the beginnings of two very different modes of growth:

(36) Wang, X.; Rodriguez, J. A.; Hanson, J. C.; Perez, M.; Evans, J. *J. Chem. Phys.* **2005**, *123*, 221101.
(37) Esch, F.; Fabris, S.; Zhou, L.; Montini, T.; Africh, C.; Fornasiero, P.; Comelli, G.; Rosei, R. *Science* **2005**, *309*, 752.
(38) Campbell, C. T.; Peden, C. H. *Science* **2005**, *309*, 713.
(39) Tibiletti, D.; Amieiro-Fonseca; Burch, R.; Chen, Y.; Fisher, J. M.; Goguet, A.; Hardcare, C.; Hu, P.; Thompsett, D. *J. Phys. Chem. B* **2005**, *109*, 22553.

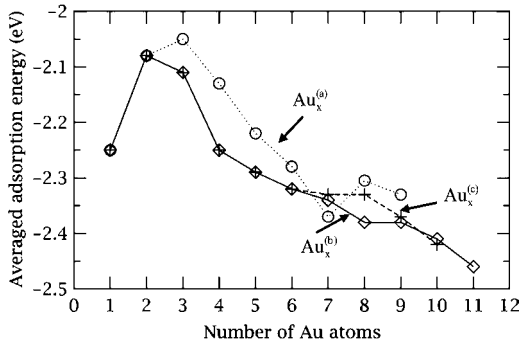

Figure 2. Averaged adsorption energies (ΔE_x^{av}), as defined in eq 1. Solid and dashed curves represent ΔE_x^{av} for the most stable structures formed via the 3D growth mechanism, namely, $Au_x^{(b)}$ and $Au_x^{(c)}$, respectively; the dotted curve represents those formed via the 2D growth mechanism ($Au_x^{(a)}$). The results for $Au_x^{(a)}$ ($x \geq 5$) are obtained in the (4×4) cell and the rest are obtained in the (3×3) cell.

layer-by-layer (2D) growth (i.e., adsorbates tend to spread at surfaces and a new atomic layer does not start until the preceding layer is complete) and three-dimensional (3D) island growth (i.e., adsorbates prefer to form multiple atomic layers). $Au_3^{(b)}$ is -0.17 eV more stable than $Au_3^{(a)}$, suggesting that the 3D island growth may be preferred. The comparison between the two mechanisms is made in Figure 2, where the solid and dotted curves represent results for those structures formed via the 3D island and 2D layer-by-layer growth modes, respectively. As will be seen later, the 3D growth becomes more favorable in general.

Upon the arrival of the fourth Au atom, many possible configurations of Au_4 can be envisaged. It gradually becomes clear that it would be a formidable task to exhaust all possibilities, particularly when the cluster becomes much larger. Thus, in the following we choose several most stable and most representative configurations of Au_{x-1} and subsequently search for stable configurations for the xth Au atom. On the basis of the two most stable Au_3 clusters, we identify two Au_4 clusters, one of which [$Au_4^{(a)}$] follows the layer-by-layer mechanism and the other of which [$Au_4^{(b)}$] follows the 3D island growth mode. In the most stable configuration [$Au_4^{(b)}$], the fourth Au atom sits above the other three Au atoms, forming a pyramidal structure; only one of the basal Au atoms (the first) occupies the vacancy site. Note that, in $Au_4^{(b)}$, the first Au atom has some lateral geometrical shifts toward the rest of the Au atoms, reflecting the significant Au−Au bonding.

Formations of Au_5 and Au_6 exhibit similar features: the pyramidal geometry is largely preserved in the 3D island growth [$Au_5^{(b)}$and $Au_6^{(b)}$], and the pyramidal geometries are more stable than the structure that tends to spread over the surface. Another salient feature in $Au_5^{(b)}$and $Au_6^{(b)}$ is that the first Au atom, initially at the O vacancy site, moves significantly away from the surface: with respect to the surface O atoms, the vacancy-adsorbed Au atom now sits more than 2.0 Å higher. As a result, the first Au atom even protrudes ~0.5 Å beyond its adjacent Au atoms that are attached to the surface O atoms. As will be seen, this feature remains for the larger clusters. For the convenience of discussion, we will henceforth use the phrase "the first-layer Au" to refer to the first Au atom and all other Au atoms that directly bond to the surface. We note that the upward shift of the first Au atom also occurs in $Au_x^{(a)}$ ($x \geq 3$). This is because in $Au_3^{(a)}$, for example, the first Au atom bonds to two other Au atoms at edges while the latter Au atoms themselves must also bond with their neighboring surface O atoms (Figure 1). Such a bonding structure means that the first Au atom cannot be accommodated at its original vacancy position, because the resulting Au−Au distances would be a little too large to be stable. Therefore, it is the intrinsic surface structure that is mainly responsible for the upward movement of the first Au atom.

As the cluster grows larger, it is necessary to examine the finite size effects in our calculations. To this end, we calculate the 2D clusters [$Au_5^{(a)}$and $Au_6^{(a)}$] in the larger (4×4) unit cell, which are reported in Figure 2. We find that while the geometrical features remain almost the same in the calculations conducted in the two cells, the adsorption energies become more negative by 0.02 and 0.03 eV in the (4×4) cell for $Au_5^{(a)}$ and $Au_6^{(a)}$, respectively. Despite the noticeable energy differences, the 2D clusters are still less stable than their 3D counterparts [$Au_5^{(b)}$ and $Au_6^{(b)}$], as can be seen from Figure 2, where the adsorption energies for $Au_x^{(a)}$ ($x \geq 5$) in the (4×4) cell are shown. Furthermore, the 3D clusters in the (4×4) cell would also have somewhat more negative adsorption energies due to the similar finite size effect, which means that the 3D clusters would be even more stable than the 2D counterparts (see also Supporting Information, where the calculations with PBEsol are carried out in the 4×4 cell). Hence, we did not attempt to calculate those 3D clusters in the larger cell.

Moving to Au_7, we display three structures in Figure 1. In addition to the 2D structure that tends to spread over the surface [$Au_7^{(a)}$], we also identify two other configurations [$Au_7^{(b)}$ and $Au_7^{(c)}$], both falling into the category of 3D island growth mode. The $Au_7^{(b)}$ and $Au_7^{(c)}$ clusters have very similar energies but differ only by the numbers of first- and second-layer Au atoms; such is also often true for larger clusters. ΔE_x^{av} for $Au_7^{(c)}$ is shown in the dashed curve in Figure 2. An interesting feature at $x = 7$ is that the 2D cluster [$Au_7^{(a)}$] appears to be slightly more stable than the 3D ones: $Au_7^{(a)}$is ~0.03 eV more stable than $Au_7^{(b)}$ in Figure 2, where the result for the latter is obtained in the (3×3) cell; $Au_7^{(a)}$ is ~0.01 eV more stable than $Au_7^{(b)}$when the latter is calculated in the (4×4) cell (not shown). This feature can be also seen from the PBEsol results in Supporting Information. Furthermore, $Au_7^{(a)}$ is even more stable than $Au_8^{(a)}$, although the latter is indeed less stable than its 3D counterpart, as shown in Figure 2. The result that $Au_7^{(a)}$ is particularly stable may be understood from its peculiar geometry. In $Au_7^{(a)}$, each of the six Au atoms at edges bonds with three other Au atoms and one surface O atom; either removing or adding one Au atom would result in some less-coordinated Au atoms [i.e., those in $Au_6^{(a)}$and $Au_8^{(a)}$], thus reducing the overall stability. In $Au_7^{(b)}$, on the other hand, the Au atom at the second layer forms three Au−Au bonds, but it loses the bond with a surface O atom compared to the situation in $Au_7^{(a)}$.

From Figure 2, $Au_9^{(a)}$ is more stable than $Au_8^{(a)}$ but clearly less stable than $Au_9^{(b)}$or $Au_9^{(c)}$, even though the results of the 3D clusters are obtained in the (3×3) cell. We therefore considered that it was not necessary to calculate the 3D clusters in the larger cell. We did not investigate any larger 2D clusters in the (4×4) cell either, as the effect of finite cell size would become significant. For the 3D island growth, we could add one more Au atom on top of $Au_{10}^{(b)}$ to create $Au_{11}^{(b)}$, because the addition is along the ⟨111⟩ direction, causing no significant lateral repulsion between cells. However, any further addition to $Au_{11}^{(b)}$ or $Au_{10}^{(c)}$ in the (3×3) cell would result in a less stable cluster.

3.2. Stabilities of the 3D Clusters. From Figure 2, the 3D island growth mechanism is clearly more favorable than the layer-by-layer one (with the exception of Au_7), owing to the

fact that the Au−Au bonding is much stronger than the Au−O bonding. Figure 2 also suggests a trend for ΔE_x^{av} in the 3D growth mechanism: with the exception of $Au_1 \rightarrow Au_2$, ΔE_x^{av} decreases monotonically with increasing number of Au atoms. This is plausible, since ΔE_x^{av} is defined to be the energy gain with respect to the isolated Au atom and the pure surface, and the adsorption of an isolated Au atom would tend to lower the total energy of the system due to new bond formation. As many Au atoms are largely undercoordinated in Au_{10} (or Au_{11}) clusters, adsorption of more Au atoms is likely to further lower ΔE_x^{av}. Eventually, ΔE_x^{av} should approach the cohesive energy for bulk Au (−3.03 eV),[40] which may be viewed as the upper limit of the averaged Au adsorption energy. A question therefore arises as to whether the clusters obtained are realistic sizes of clusters for the ceria surface.

We answer the above question from the following three aspects. We first note that Au nanoclusters reported in experiments have varied sizes, ranging from ∼1 to ∼6 nm in diameter.[1,4,13,14] For example, Fu et al.[1] reported that Au species on ceria, which are active for the WGS reaction, have a mean particle size of ∼5 nm; with X-ray techniques, however, Tibiletti et al.[39] suggested that the active Au cluster is much smaller, containing about 50 atoms (2−3 nm). The uncertainty of the nanoparticle size in experiments is not surprising, as both active and inactive species could coexist; active species could take different forms; and active species could also be beyond the resolution limit of some techniques. Interestingly, Herzing et al.,[41] using state-of-the-art scanning transmission electron microscopy, which is an ideal instrument to examine species present in highly active samples, showed recently that the active Au nanoclusters, on iron oxides, were identified to be ∼0.5 nm, containing only ∼10 atoms. Thus, we consider that small and active Au clusters are also likely to be present on ceria. Clearly, it is highly desirable that the same experimental technique is applied on Au/ceria systems to clarify the issue. Second, we also note that entropic effects could become important at moderate and high temperatures in assessing the relative stability of these clusters and the bulk limit, in particular, the configurational contribution. In view of the uncertainties surrounding the choices of the precise number of vacancies and clusters, and of the sizes of vacancy and clusters, we do not attempt to calculate this entropy. Qualitatively, however, one would expect that the smaller clusters present more ways of arranging themselves on a given number of oxygen vacancy sites than the larger clusters. In other words, the effect from the configurational entropy would favor the formation of smaller clusters. Third, even if the clusters thus obtained are indeed thermodynamically unfavorable compared to larger clusters or the bulk limit, they could still be kinetically viable. To demonstrate the kinetic stability, we carried out molecular dynamics (MD) calculations on $Au_{11}^{(b)}$ and $Au_{10}^{(c)}$ at a constant temperature $T =$ 1000 K. This high temperature was chosen so that we can assess the kinetic stability of the two systems subject to a large thermal fluctuation. The time step used in the MD simulation was 0.1 fs: the small time step was chosen because of the difficulty in the electronic optimization at larger time steps. In a total of ∼8 ps of MD simulation, no new configuration has been found and the characteristic geometries of $Au_{11}^{(b)}$ or $Au_{10}^{(c)}$ have remained unchanged.

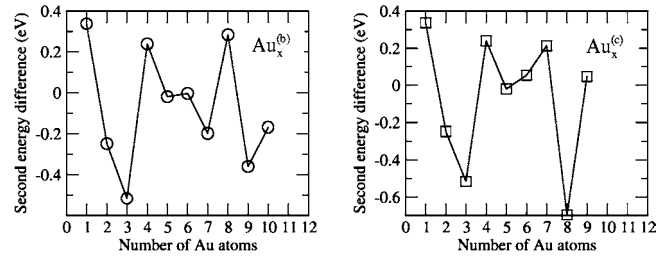

Figure 3. Second energy difference (δE_x), as defined in eq 2, for $Au_x^{(b)}$ (left) and $Au_x^{(c)}$ (right).

Returning to Figure 2, we continue to discuss the relative stability of $Au_x^{(b)}$ and $Au_x^{(c)}$ at a given x. As briefly mentioned in the last section, $Au_x^{(b)}$ and $Au_x^{(c)}$, in general, have quite similar energies; for example, ΔE_x^{av} for $Au_{10}^{(b)}$ and $Au_{10}^{(c)}$ differs by less than 0.01 eV. The only relatively large difference lies at $x = 8$: ΔE_x^{av} for $Au_8^{(c)}$ is 0.05 eV less negative than that for $Au_8^{(b)}$. This may be understood from the less favorable structure in the former cluster. Compared to $Au_8^{(b)}$, more Au atoms are present in the second-layer of $Au_8^{(c)}$, which would have to form bonds with fewer first-layer Au atoms. Thus, significant bonding competition would occur among the second-layer Au atoms, and consequently these atoms do not adsorb directly above the 3-fold hollow site of the first layer (i.e., the most stable adsorption site), as can be seen from Figure 1.

Sometimes, however, one also needs to consider the relative stability of clusters with differing numbers of atoms. A good example is the study of the so-called magic number for some metal clusters: those metal clusters with the magic number of atoms are particularly stable.[42,43] The relative stability of clusters with different numbers of atoms is difficult to extract from the results of ΔE_x^{av} alone. Instead, a so-called second energy difference (δE_x) is often used in the literature for this purpose,[44] given by

$$\delta E_x = E_{slab}^{Au_{x+1}} + E_{slab}^{Au_{x-1}} - 2E_{slab}^{Au_x} \qquad (2)$$

where the terms on the right-hand side are energies of Au_{x+1}/CeO_2, Au_{x-1}/CeO_2, and Au_x/CeO_2, respectively. Here, as is well-known, δE_x is the relative binding energy of a cluster with x atoms with respect to those with $x + 1$ and $x - 1$ atoms. When δE_x is plotted, therefore, its peaks represent relatively more stable clusters. We show δE_x in Figure 3 for the two 3D cluster sequences. Clearly, for $Au_x^{(b)}$, Au_4, and Au_8 are the relatively more stable clusters; for $Au_x^{(c)}$, Au_4, and Au_7 are the relatively more stable clusters.

The existence of those magic numbers (4, 7, and 8) may also be understood from the geometries of the corresponding clusters. Let us take $Au_4^{(b)}$ as an example; other cases can be rationalized in a similar fashion. As can be seen from Figure 1, every Au atom in $Au_3^{(b)}$ is less coordinated than that in $Au_4^{(b)}$, and the newly arrived Au atom in $Au_5^{(b)}$ [from $Au_4^{(b)}$] is much less coordinated than the rest of the Au atoms. In other words, Au atoms in $Au_4^{(b)}$ are more saturated than those in $Au_3^{(b)}$ or $Au_5^{(b)}$, and thus the former is more stable.

3.3. Geometries, Packing Orders, and Facets of the Nanoclusters. Clear and characteristic regular geometrical features emerge in the larger clusters, which may be related to close-packed bulk

(40) Zhang, C.; Alavi, A. *J. Am. Chem. Soc.* **2005**, *127*, 9808.
(41) Herzing, A. A.; Kiely, C. J.; Carley, A. F.; Landon, P.; Hutchings, G. J. *Science* **2008**, *321*, 1331.
(42) Knight, W. D.; Clemenger, K.; de Heer, W. A.; Sauders, W. A.; Chou, M. Y.; Cohen, M. L. *Phys. Rev. Lett.* **1984**, *52*, 2141.
(43) Neukermans, S.; Janssens, E.; Tanaka, H.; Silverans, R. E.; Lievens, P. *Phys. Rev. Lett.* **2003**, *90*, 033401.
(44) Harbola, M. K. *Proc. Natl. Acad. Sci. U.S.A.* **1992**, *89*, 1036.

structures. In $Au_{11}^{(b)}$ and $Au_{10}^{(c)}$, for instance, we see that the atoms of each successive layer occupy 3-fold hollow sites formed by the layer beneath. In fact, these clusters are *just* large enough for us to identify the beginnings of a face-centered cubic (fcc) structure in $Au_{10}^{(c)}$ (i.e., ABC stacking) and of a hexagonal close-packed (hcp) structure in $Au_{11}^{(b)}$ (i.e., ABA stacking). Taken to the extreme of a sufficiently large cluster, we would expect the fcc geometry to be energetically favored, since the bulk cohesive energy of Au in the cubic arrangement is calculated by us as 3.03 eV, whereas for the hexagonal arrangement it is 2.98 eV. These values are sufficiently close, however, to suggest that the case may not be entirely clear-cut for very small clusters. Indeed, for the clusters studied here, the $Au_x^{(b)}$ and $Au_x^{(c)}$ examples generally have very similar binding energy per atom for any given x large enough to distinguish between the two types of geometry; moreover, where a notable difference does occur, for $x = 8$, it is the (b) geometry that is favored over the (c) geometry (i.e., the proto-hcp is favored over the proto-fcc). Clearly it would be desirable to conduct calculations for rather larger clusters, to determine over what range of sizes the fcc and hcp structures are competitive. Unfortunately, the computational cost of doing so is currently prohibitive, so we must resort to plausibility arguments. Extrapolating the curves in Figure 2 toward higher x, on the basis of the approximate linearity observable between $x = 4$ and $x = 11$, we estimate that the bulk cohesive energy would be reached at cluster sizes in the vicinity of 35 Au atoms. If the actual approach to bulklike behavior is more asymptotic than abrupt, then it is reasonable to assume that the cluster energies differ considerably from those of the bulk until *at least* this size is reached. In Figure 4, we show a variety of different plausible clusters showing either fcc-like or hcp-like stacking within this size range. In the fcc-like clusters, we suggest that the exposed facets are likely to be of {111} character [similar to those exposed in the $Au_{10}^{(c)}$ cluster] or of {100} character (similar to those observed experimentally for larger clusters[13]). For the hcp-like clusters, we propose that exposed facets are likely to be of $\{10\bar{1}1\}$ character [as found in our calculated $Au_{11}^{(b)}$ cluster] or of {0001} character (typically the lowest energy surface for hexagonal metals). Incidentally, the {0001} and $\{10\bar{1}1\}$ surfaces are notable as being, respectively, the only flat hcp surface and the simplest stepped hcp surface after $\{10\bar{1}0\}$.[45]

Another interesting point of note is the size evolution of Au−Au bond distances. As shown in experiments,[46,47] the interatomic distance decreases as the cluster size decreases. Although the sizes of the clusters in the experiments are generally larger than those in our simulations, we find that this trend still appears to be true in our relatively small clusters. Figure 5 displays the average length of the Au−Au bonds, which is often used for this purpose,[48,49] for each of the most stable Au clusters [i.e., the $Au_x^{(b)}$ series]. As can be seen, the Au−Au bond distance increases in general (with the exception of Au_3 and Au_4) with increasing size of the clusters. A closer look at $Au_3^{(b)}$ and $Au_4^{(b)}$ reveals that the longer Au−Au bond distances in the clusters always involve the first Au atom that adsorbs at the O vacancy site. This is because the first Au atom sits in a significantly lower position than the rest of the Au atoms, the latter being bonded with O atoms at the surface top layer. This feature disappears from $Au_5^{(b)}$, because the vacancy-absorbed Au moves upward with respect to the surface, as discussed earlier.

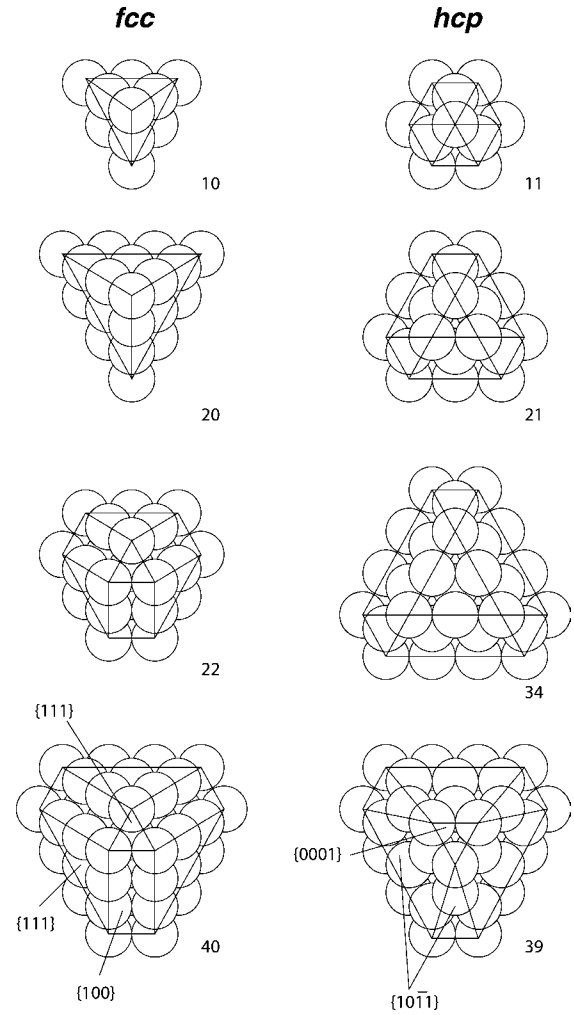

Figure 4. Possible fcc and hcp geometries of Au nanoclusters, with exposed planes marked in the largest cases. Additional numerals adjacent to each cluster indicate the number of Au atoms.

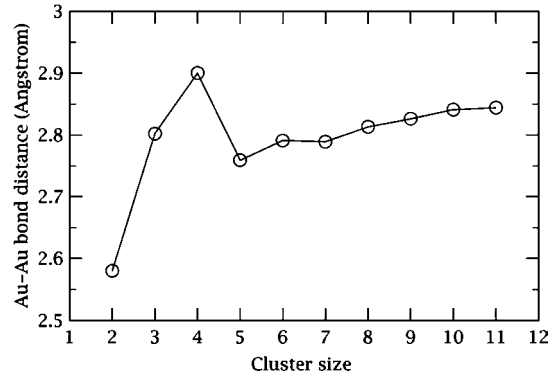

Figure 5. Average length of Au−Au bonds in $Au_x^{(b)}$ ($x = 2-11$).

3.4. Electronic Analysis. We first discuss the Au oxidation state. This is because the Au oxidation state links closely to the catalytic activity for the WGS reaction, and there is also a vigorous debate on the nature of the active form of gold, i.e. whether it is cationic or metallic, in the literature.[4] Thus, it would be interesting to examine what oxidation state those Au clusters

(45) Pratt, S.; Jenkins, S. J. *Surf. Sci. Rep.* **2007**, *62*, 373.
(46) Miller, J. T.; Kropf, A. J.; Zha, Y.; Regalbuto, J. R.; Delannoy, L.; Louis, C.; Bus, E.; van Bokhoven, J. A. *J. Catal.* **2006**, *240*, 222.
(47) Balerna, A.; Bernieri, E.; Picozzi, P.; Reale, A.; Santucci, S. *Surf. Sci.* **1985**, *156*, 206.
(48) Wang, J.; Wang, G.; Zhao, J. *Phys. Rev. B* **2002**, *66*, 035418.
(49) Fa, W.; Luo, C.; Dong, J. *Phys. Rev. B* **2005**, *72*, 205428.

Table 1. Au Charges (e) in Various Au Clusters[a]

	1st	2nd	3rd	4th	5th	6th	7th	8th	9th	10th	11th	$n_{Ce^{3+}}$	e_t	e_d
Au_1	−0.62											1	−0.62	0.062
Au_2	−0.36	+0.09										2	−0.27	0.083
$Au_3^{(b)}$	−0.59	+0.09	−0.16									1	−0.66	0.052
$Au_4^{(b)}$	−0.61	+0.17	−0.08	+0.17								2	−0.35	0.059
$Au_5^{(b)}$	−0.21	+0.22	−0.04	+0.19	+0.00							3	+0.16	0.058
$Au_6^{(b)}$	−0.08	+0.17	−0.06	+0.22	+0.03	+0.14						4	+0.42	0.049
$Au_7^{(b)}$	−0.08	+0.03	−0.12	+0.14	+0.12	+0.18	−0.05					4	+0.22	0.058
$Au_8^{(b)}$	−0.10	+0.20	−0.05	+0.13	+0.02	+0.11	−0.09	+0.14				4	+0.36	0.056
$Au_9^{(b)}$	−0.02	+0.19	−0.06	+0.09	+0.07	+0.07	−0.06	+0.14	+0.03			4	+0.45	0.053
$Au_{10}^{(b)}$	−0.27	+0.14	−0.10	+0.15	+0.14	+0.14	−0.09	+0.14	+0.15	−0.09		4	+0.31	0.058
$Au_{11}^{(b)}$	−0.03	+0.17	−0.03	+0.16	+0.17	+0.17	−0.02	+0.16	+0.18	−0.03	−0.12	5	+0.78	0.042

[a] The labels of Au atoms are indicated in Figure 5. For each cluster, the total charge of Au (e_t), the number of reduced Ce ions ($n_{Ce^{3+}}$) and the d electron difference (e^d, defined as the number of d electrons per Au in each cluster subtracting the number of d electrons per Au in the bulk) are also included.

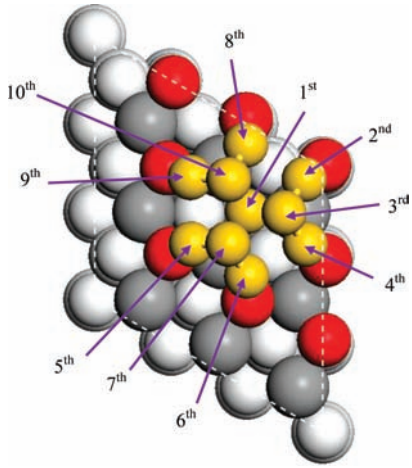

Figure 6. Labels of Au atoms in $Au_{10}^{(b)}$. The Au atoms are drawn in different sizes from those in Figure 1, so that the labels can be seen clearly.

have to offer. We summarize in Table 1 the Au charges in Au_x ($x = 1-11$), which are calculated via Bader's method.[50] For the labeling reference, we redraw $Au_{10}^{(b)}$ in Figure 6, where the Au atoms are labeled according to the sequence that they are added. As can be seen there, the first Au atom is the one from which the nucleation starts (i.e., at the original vacancy site); the second, fourth, fifth, sixth, eighth and ninth are the first layer Au atoms; the third, seventh, and tenth are the second layer Au atoms; the 11th is the third layer Au atom, which is not shown because it would block the view of the first Au atom. To simplify matters, we list just one type of cluster [i.e., $Au_x^{(b)}$ ($x = 3-11$)] in Table 1 [the other type of cluster (i.e., $Au_x^{(c)}$ ($x = 7-10$)] shows the same qualitative picture). Table 1 also includes the total charge of our Au clusters and the number of Ce ions reduced upon Au adsorption.

Several interesting results can be seen from Table 1. First, the first Au atom is always negatively charged (i.e., $Au^{\delta-}$). As shown in our previous study and others, at the reduced surface with an O vacancy, the two excess electrons left behind by the removed O would localize on two Ce ions and the partially occupied f states sit just below the Fermi level.[7,16,32-34] Upon the adsorption of an Au atom, some of the electrons in the occupied f states would enter into the Au 6s state so that $Au^{\delta-}$ forms.[7,16] Second, the first Au atom in Au_{1-4} clusters is generally more negatively charged than in Au_{5-10} clusters; in fact, the *total* charges in the former have a different sign (negative) from those in the latter (positive). These features coincide with the geometries described earlier: the first Au atom more or less stays at the original vacancy site in Au_{1-4}, but it moves upward significantly in Au_{5-11}. Clearly, the upward geometrical change, induced by the strong Au−Au interaction, prevents to some extent the electron transfer to the first Au atom. Third, the remaining Au atoms in the first layer are all positively charged (i.e., $Au^{\delta+}$) in all the clusters. This result, we believe, is highly plausible. As shown in our previous study, Ce^{4+} has empty f states just above the Fermi level (i.e., able to accept electrons); when a Au atom forms bonds with an O atom at the surface, some electronic charge would transfer from Au to Ce, resulting in oxidation of Au and reduction of Ce.[16] Fourth, larger clusters generally tend to have more $Au^{\delta+}$ because more Au atoms are attached to surface O atoms, and simultaneously more Ce atoms are reduced. With the exception of Au_2, the number of Ce^{3+} ions increases from 1 to 5 with increasing cluster size. Fifth, the second-layer Au atoms are somewhat negatively charged. In $Au_{11}^{(b)}$, where the second-layer Au atoms do not constitute the outermost layer, the negative charges are very mild. This suggests that, in larger clusters, the second-layer Au atoms are more metallic than ionic.

We comment further on one of the above results: the presence of $Au^{\delta+}$ at the first Au layer just above the surface. Although our clusters are small, we expect that this electronic feature is likely to be true in much larger clusters: as the first-layer Au atoms bond directly with the surface, electron transfer to the surface could always readily occur; moreover, Table 1 shows that the positive charges of the first-layer Au atoms are rather insensitive to the increase in total number of Au atoms. More importantly, we consider that the presence of $Au^{\delta+}$ at the first Au layer could have important implications in catalysis. As shown previously,[7] in the WGS reaction, CO would preferentially adsorb at $Au^{\delta+}$ rather than anionic or metallic Au, because the bonding involving 5σ (CO) donation to 6s (Au) benefits from an empty 6s orbital, as in $Au^{\delta+}$. Hence, we expect that CO adsorption would most likely occur at the first-layer Au atoms. In other words, $Au^{\delta+}$ still has an important catalytic role to play, even when the majority of Au atoms in each cluster are metallic or negatively charged. Another point of note is that $Au^{\delta+}$ obtained at the reduced surface in this work is generally charged to around +0.1e to +0.2e. This is clearly different from either the pure Au cluster without the support, where metallic Au is expected, or the Au cluster model based on a Ce vacancy site where the Au that substitutes the Ce is very strongly positively charged (+1.2e), or even Au at the perfect surface,

(50) Bader, R. F. W. *Atoms in Molecules: A Quantum Theory*; Clarendon: Oxford, U.K., 1990.

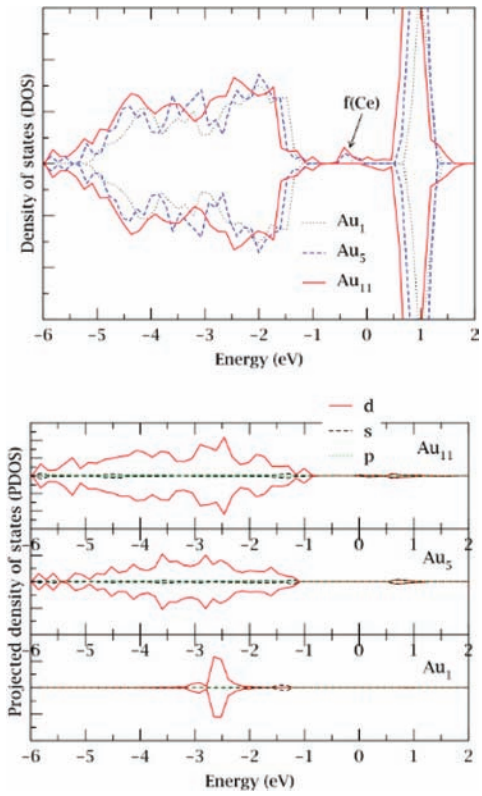

Figure 7. Total density of states (DOS) (top) and the DOS projected onto Au s, p, and d orbitals (bottom) of Au_1, $Au_5^{(b)}$, and $Au_{11}^{(b)}$. A Gaussian broadening of 0.05 eV is used. The Fermi levels of each system are aligned and set to 0.

where Au sits at an O bridgelike site with a charge of +0.32e.[16] We believe that there will be different CO−Au bonding strengths in these various situations. Clearly, this difference would have significant implications in determining the reaction mechanisms.

We also plot in Figure 7 the total density of states (DOS) of several representative clusters [$Au_1^{(b)}$, $Au_5^{(b)}$, and $Au_{11}^{(b)}$] and the total DOS projected onto Au s, p, and d oribtals. As can be seen, increasing size of the cluster increases the interaction between Au atoms and consequently the width of d-bands (i.e., d states appear at both lower and higher energy levels). This agrees with previous DFT calculations on pure Au clusters.[48] On the other hand, increasing the size of the cluster increases the occupancy of the f (Ce) orbitals, as indicated in the DOS. This is because the original empty f orbitals of Ce^{4+}, which are just above the Fermi level,[16] now accept electrons from Au atoms, as discussed above. We also note that the Au d states closest to the Fermi level (e.g., ~ -1.0 eV) in the larger cluster are largely due to the Au atoms at the contact layer. This result therefore lends further support to above suggestion that the contact-layer Au atoms, which are positively charged, should be relatively more active.

Experimentally, below about 3 nm, the number of d electrons was observed to be greater than in bulk Au in the XANES spectra.[46] It is therefore interesting to examine the behavior of d electrons in our clusters. We calculate the number of d electrons by integrating the occupied DOS projected onto the Au d orbitals. In order to compare with the XANES result, we subtract the number of d electrons per Au in the bulk from the number of d electrons per Au in each cluster and compile the result (denoted as e_d) in Table 1. As can be seen, the number of d electrons in the clusters is indeed larger than that in the bulk, consistent with the experiment, although there is no evident trend within the clusters themselves. The enrichment of d electrons in the clusters may be understood from the fact that the relatively small Au−Au distance in the clusters (compared to the bulk) increases the overlap of d-bands and lowers the energies of d-bands, which makes more d occupancy favorable.

4. Conclusion

There is a clear need to understand the structure of Au clusters on ceria, which is relevant to investigations of their catalytic properties and to clarification of reaction mechanisms. By depositing Au atoms one by one at the ceria surface, this work examines the initial Au nucleation. From the clusters obtained, we identify both fcc and hcp packing features. Where we have been able to do the calculation, the fcc-like and hcp-like clusters have similar energies, with the latter situation favored, if anything. Ultimately, however, the fcc-like stacking must be favored for the largest clusters. We speculate that fcc/hcp polymorphism may be exhibited for cluster sizes up to around 35 Au atoms. Although these are not likely to be thermodynamically favorable (compared to the bulk), they may be kinetically stable and potentially highly relevant to catalysis. From an electronic standpoint, we find that contact-layer Au atoms that form bonds with surface O atoms are probably charge-positive, even when overlaid by other Au atoms within a large cluster. The importance of positively charged Au to catalysis need not, therefore, be limited to ultrasmall clusters.

Acknowledgment. We acknowledge the Cambridge Isaac Newton Trust (C.Z.) and The Royal Society (S.J.J). A.M. is supported by the EURYI scheme (see www.esf.org/euryi), the European Research Council, and the EPSRC.

Supporting Information Available: Additional material as described in the text. This material is available free of charge via the Internet at http://pubs.acs.org.

JA906687F